

Turbulent magnetic fields in the quiet Sun: implications of *Hinode* observations and small-scale dynamo simulations

Jonathan Pietarila Graham, Sanja Danilovic, and Manfred Schüssler

Max-Planck-Institut für Sonnensystemforschung, 37191 Katlenburg-Lindau, Germany

ABSTRACT

Using turbulent MHD simulations (magnetic Reynolds numbers up to ≈ 8000) and *Hinode* observations, we study effects of turbulence on measuring the solar magnetic field outside active regions. Firstly, from synthetic Stokes V profiles for the FeI lines at 6301 and 6302 Å, we show that a peaked probability distribution function (PDF) for observationally-derived field estimates is consistent with a monotonic PDF for actual vertical field strengths. Hence, the prevalence of weak fields is greater than would be naively inferred from observations. Secondly, we employ the fractal self-similar geometry of the turbulent solar magnetic field to derive two estimates (numerical and observational) of the true mean vertical unsigned flux density. We also find observational evidence that the scales of magnetic structuring in the photosphere extend at least down to an order of magnitude smaller than 200 km: the self-similar power-law scaling in the signed measure from a *Hinode* magnetogram ranges (over two decades in length scales and including the granulation scale) down to the ≈ 200 km resolution limit. From the self-similar scaling, we determine a lower bound for the true quiet-Sun mean vertical unsigned flux density of ~ 50 G. This is consistent with our numerically-based estimates that 80% or more of the vertical unsigned flux should be invisible to Stokes- V observations at a resolution of 200 km owing to the cancellation of signal from opposite magnetic polarities. Our estimates significantly reduce the order-of-magnitude discrepancy between Zeeman- and Hanle-based estimates.

Subject headings: Sun: magnetic fields — turbulence — MHD — techniques: polarimetric

1. Introduction

Determining the strength of the magnetization of the “quiet” Sun is tied to the question of how much flux resides at small scales. This is important, for example, in determining

the energy budget available for chromospheric heating. Observationally, two methods are employed to constrain the solar magnetic field: the Hanle and Zeeman effects. The Hanle effect measures (in principle) the mean magnetic field strength, $\langle |B| \rangle$, as there are no cancellation effects, but quantitative interpretation requires assumptions about the probability distribution function (PDF) of the turbulent magnetic field. The Hanle de-polarization is measured in stronger lines formed in the mid- to upper-photosphere and estimates are made of $\langle |B| \rangle \sim 130$ G, the field residing primarily in the intergranular lanes (Trujillo Bueno et al. 2004). The Zeeman effect measures the longitudinal component (via Stokes V) and transverse components (via Stokes Q and U) of the magnetic field but suffers from cancellation effects. Hence, it is “blind” to any “hidden” mixed-polarity flux at scales smaller than the resolution limit of an instrument. However, the benefit of Zeeman measurements is that their interpretation requires no assumption about the turbulent PDF and measurements can actually be used to determine the PDF on scales larger than the resolution limit. Some attempts to incorporate the effects of cancellation into Zeeman-based Stokes inversions utilize the micro-structured field hypothesis (Sanchez Almeida et al. 1996). However, typical estimates based on the longitudinal Zeeman effect give $\langle |B_z| \rangle \sim 10$ G for the mean unsigned vertical flux density (see Table 3 in Bello González et al. 2009 for a review of the spread of recent Zeeman-based estimates). These values are significantly smaller than the Hanle-based estimates. The discrepancy between the results from Hanle (~ 100 G) and Zeeman (~ 10 G) measurements is not unexpected since the Zeeman observations see only the resolved flux while the Hanle interpretation depends on assumptions about an unknown PDF.

In this work, we ask the question “How can the turbulent fractal geometry of the magnetic field in the solar photosphere be accounted for in interpretations of Zeeman-based observations?” We attempt to derive the spectral/fractal properties from high resolution ($0''.3$) Zeeman observations with the *Hinode* spectro-polarimeter (SP) (Kosugi et al. 2007; Tsuneta et al. 2008; Lites et al. 2001) and high resolution (down to $4\text{ km} \approx 0''.006$), turbulent dynamo simulations (up to magnetic Reynolds numbers, $Re_M \approx 8000$) with the MURaM code (Vögler 2003; Vögler et al. 2005). First, we clarify the consistency of PDFs derived from observations and simulations, respectively. Zeeman observations typically show PDFs of quantities derived from Stokes V which can be described as a peaked function (Khomenko et al. 2005; Lites et al. 2008b). We demonstrate that the peaked PDFs from Stokes V measurements and the monotonic PDFs typically reported from numerical simulations are, in fact, compatible. Failure to take into account this observational bias can lead to a gross underestimation of the prevalence of weak fields and, consequently, to incorrect estimates of the mean magnetic field strength and magnetic energy density in the solar photosphere.

Second, we extrapolate the results obtained with observations and simulations (based

on their respective fractal properties) to scales below the resolution limits to estimate the amount of “hidden” flux. To do this, we exploit the fact that the fractal geometry is intimately connected to power-law scaling relations such as $N(l) \propto l^{-D_f}$. Here, $N(l)$ is the number of boxes of edge length l covering a fractal set (such as all pixels with apparent magnetic flux above some threshold) and D_f is the fractal dimension. It has long been known that the distribution of plage magnetic field is such a statistically self-similar fractal (Schrijver et al. 1992; Balke et al. 1993). As the threshold can influence the fractal dimension inferred, however, the geometrical structure is more complicated than a simple fractal. In this case, the fractal concept must be generalized by adding a measure defined by the absolute value of the net magnetic flux through each box of edge length l . This measure also displays self-similarity (a power-law scaling) for the solar quiet Sun network magnetic flux (down to $0''.5$ resolution in Lawrence et al. 1993 and Cadavid et al. 1994; see also Krivova & Solanki 2004) and also for numerical simulations of magnetoconvection (Brandenburg et al. 1992). Hence, the geometry of the magnetic field is said to be multifractal.

Cancellation effects do not play an important role in observations of the multifractal unipolar solar regions discussed above. In contrast, if the magnetic field of the quiet Sun internetwork is multifractal (as we will show), cancellation can play a significant role for scales below $1''$ (see also Sánchez Almeida et al. 2003). For these mixed-polarity fields it is necessary to further generalize the fractal concept to a signed measure. Here, the power-law scaling exponent is the cancellation exponent (Ott et al. 1992). If this self-similar power-law scaling extends below the observational resolution, small scale cancellation will occur and correct values of the mean field strength and energy cannot be established. As was pointed out by Lawrence et al. (1993), such a signed measure could also be employed to extrapolate moments of the magnetic field below resolvable limits. Until now, no attempt has been made to employ self-similar scaling to estimate the total cancellation, and, hence, the true mean quiet-Sun magnetic field strength.

2. Data and Methods

We use MURaM simulations (Vögler 2003; Vögler et al. 2004, 2005) for a rectangular domain of horizontal extent $4.86 \times 4.86 \text{ Mm}^2$ and a depth of 1.4 Mm . Runs of small-scale, local dynamo action with increasing resolution and Reynolds numbers have been carried out (see Table 1). The turbulence is sufficient for small-scale dynamo action (Vögler & Schüssler 2007). All magnetic field in the simulations results from dynamo amplification of a small seed field as there is no net flux through the box, no flux advected into the box, and no initial large-scale field. A well-known rule-of-thumb for forced turbulence simulations is that

one decade of scales smaller than the forcing is required before the inertial range begins and another decade is required (at the opposite end of the spectrum) for the dissipative scales. For photospheric magneto-convection simulations, where the forcing granulation scale is 1 Mm, this means that a grid resolution of 10 km or smaller is required before a simulation becomes turbulent. (See Sánchez Almeida et al. (2003) for a study with a 10km resolution using a Boussinesq simulation and multi-component Milne-Eddington line synthesis.) As we compute simulations down to a grid resolution of 4 km, we are now able to measure the effects of turbulence on observational quantities.

To this end, we require synthetic profiles (for the FeI lines at 6301.5 Å and 6302.5 Å) as calculated from a snapshot of a run with non-grey radiative transfer. Owing to the computational expense of such a run, it was started from a snapshot from the statistically stationary state of Run C (see Table 1) and then run for approximately one convective turnover time, 10 minutes. Stokes V , Q , and U profiles were then computed in one dimension (1D) assuming local-thermodynamic-equilibrium (LTE) and using the `STOPRO` code in the `SPINOR` package (Solanki 1987; Frutiger et al. 2000). We will concentrate in this work, however, on Stokes V observations (and synthetic observations) at disk center. This allows us to avoid line-of-sight effects, to identify the longitudinal component of the magnetic field as its vertical component, and to avoid the difficult estimation of the cancellation properties of Stokes Q and U .

Observational data is obtained from the spectro-polarimeter (SP, Lites et al. 2001) of the Solar Optical Telescope (SOT, Tsuneta et al. 2008) on the *Hinode* satellite (Kosugi et al. 2007). One set, a spatial map, consists of 2048 scans taken on March 10, 2007 (11:37:36 – 14:36:48 UT), in the “normal mode” (exposure time of 4.8 s) with the scanning step of 0.1476'' and pixel size along the slit of 0.1585''. The data set covers a quiet Sun region at the disk center, over the large field of view of 324'' × 164''. The second set, a “deep mode” time series, consists of a 103 steps at disk center, each with an effective exposure time of 67.2 s after application of a temporal running mean, and was taken on February 27, 2007 (00:20 – 02:20 UT). Both data sets have previously been described in Lites et al. (2008b). Corrections for various instrumental effects are made using the `SolarSoft`¹ procedure `sp_prep` which calculates the wavelength-integrated Stokes V (V_{tot}),

$$V_{\text{tot}} = \text{sgn}(V_b) \frac{|\int_{\lambda_b}^{\lambda_0} V(\lambda) d\lambda| + |\int_{\lambda_0}^{\lambda_r} V(\lambda) d\lambda|}{I_c \int_{\lambda_b}^{\lambda_r} d\lambda}, \quad (1)$$

where $\text{sgn}(V_b)$ is the sign of the blue peak, λ_0 is the line center, and $\lambda_{r,b} = \lambda_0 \pm 30$ pm (Lites et al. 2008b). The procedure includes also a Milne-Eddington-based calibration of the

¹<http://www.lmsal.com/solarsoft/>

sum of V_{tot} from both lines into a measure of longitudinal “apparent flux density”, B_{app}^L (Lites et al. 2008a). This calibration is tailored to retrieve the field value from weak and noisy internetwork signals. It assumes that magnetic structures are spatially resolved (fill the resolution element) and does not take into account the magnetic field variations over the height range where lines are formed. Consequences of the latter assumption are studied in the next section, when B_{app}^L , obtained from Stokes V profiles synthesized from simulations, is compared with the vertical component of the actual magnetic field.

3. Results

3.1. PDFs

A marked difference exists between the PDFs inferred from Zeeman polarimetry (e.g., Khomenko et al. 2005; Lites et al. 2008b) and the PDFs from numerical computations (e.g., Socas-Navarro & Sánchez Almeida 2003; Vögler & Schüssler 2007). For example, in Fig. 1 we present the PDFs from the *Hinode* “normal mode” map magnetogram (apparent vertical magnetic flux density, dashed line) and of MURaM simulation Run C-NG (average vertical magnetic field, solid line). The polarimetric observation peaks at $B_{\text{app}}^L \approx 3$ G while the simulation possesses a monotonic distribution without a distinct maximum: there exists a greater amount of weak vertical field than indicated by the observations. The observation also shows greater intermittency (the distribution has an enhanced strong signal (field) tail when compared to a Gaussian) than the simulation. This can possibly be attributed to the much lower Reynolds number of the numerical simulation compared to the Sun as well as to the smaller simulation box: contributions from dynamo action in the deeper layers and supergranular network flux concentrations are absent. To address the qualitative difference (peaked versus monotonic) between simulations and observations, we ask what PDF of Zeeman-based observational signatures would result if $\text{PDF}(B_z)$ monotonically decreases with increasing vertical field strength (instead of possessing a peak). Our approach will be to assume the distribution of field strengths from turbulent MURaM simulations and examine the consequences of such a distribution on Stokes V observations.

Though noise, resolution, and other instrumental factors are important in any real observation, we first address the question assuming a “perfect” instrument. Using the synthetic profiles from Run C-NG, we calculate V_{tot} with Eq. (1) and determine B_{app}^L following Lites et al. (2008b). In Fig. 2, the derived B_{app}^L signal versus B_{ave} , the vertical magnetic field strength averaged over the height range corresponding to $\log \tau \in [-3.5, .1]$, is shown. This quantity was selected for its linear Pearson correlation with B_{app}^L of $r = 0.92$ and its co-

efficient of linearity, $B_{\text{app}}^{\text{L}} \approx 1.0 B_{\text{ave}}$, which is consistent with the calibration of Lites et al. (2008b). This height range also encompasses most of the formation height of the FeI lines at 6301 and 6302 Å. Though $B_{\text{app}}^{\text{L}}$ and B_{ave} are well correlated, there is a large scatter. We note, also, that changing the range to $\log \tau \in [-2, .1]$ does not significantly affect the correlation, r . This indicates that most of the Stokes V signal is generated in deeper layers (Orozco Suárez et al. 2007).

In Fig. 1, we present a comparison between the PDFs of $B_{\text{app}}^{\text{L}}$ as derived from the synthetic Stokes V profiles (dash-dotted line) and B_{ave} (solid line). $\text{PDF}(B_{\text{ave}})$ monotonically decreases with increasing field strength while $\text{PDF}(B_{\text{app}}^{\text{L}})$ shows a peak near 1 G and a strong decline towards smaller field strengths. The PDFs for maximum Stokes V amplitude and total circular polarization are qualitatively similar to that shown for $B_{\text{app}}^{\text{L}}$. PDFs for the vertical magnetic field from different volumes and 2D cross sections from all simulation runs, chosen either by height or by optical depth, show similar PDFs to that shown for B_{ave} . That is, the monotonically decreasing distribution is a robust feature of the vertical magnetic field when sampled by geometrical height, optical depth, or by averaging over the vertical direction. The difference between observations and simulations is caused by the radiative transfer that produces circular polarization from longitudinal magnetic field.

The above result shows that caution is needed when interpreting the distribution of Stokes V signal in order to avoid a drastic underestimation of the occurrence of weak field. This caution naturally extends to moments of the distribution such as mean vertical flux density or mean vertical magnetic energy density. For example, $B_{\text{app}}^{\text{L}}$ and B_{ave} are very well correlated with a coefficient of linearity of unity, but their averages, $\langle |B_{\text{app}}^{\text{L}}| \rangle = 6.9$ G and $\langle |B_{\text{ave}}| \rangle = 5.5$ G, differ significantly. We see that an over estimation of 26% results from assuming the vertical magnetic field to have the same distribution as the signal derived from Stokes V , even in the absence of noise (note that this is close to the 20% loss found in Sánchez Almeida et al. 2003).

To understand in more detail how radiative transfer affects contribute to a peaked PDF, we examine a few selected V -profiles. Pixels with weak B_{ave} must be generating strong $B_{\text{app}}^{\text{L}}$ signals for $\text{PDF}(B_{\text{app}}^{\text{L}})$ to become peaked. Indeed, Fig. 3 shows this is the case. There are many pixels for which $|B_{\text{ave}}| < 0.1$ G while $|B_{\text{app}}^{\text{L}}| > 5$ G. On the other hand, we see that when $|B_{\text{app}}^{\text{L}}| < 0.1$ G, $|B_{\text{ave}}|$ is always less than 4 G. In Fig. 4, we examine one case of how weak B_{ave} can be associated with strong $B_{\text{app}}^{\text{L}}$. For $\tau \in [0.1, 1]$, the vertical magnetic field takes on values of tens of Gauss. In this region, there are also strong gradients (and direction reversals) for both the magnetic and velocity fields. In this case, because of the magnetic field reversal, B_{ave} is nearly zero. However, because of the velocity gradient, the

contributions to the Stokes– V profile from the positive and negative magnetic polarities are Doppler-shifted with respect to each other. For this reason, the Stokes V signal is not cancelled. This is further illustrated in Fig. 5 where we plot the mean $B_{\text{app}}^{\text{L}}$ for all pixels with $|B_{\text{ave}}| < 0.1$ G versus the strength of the vertical velocity fluctuations. There is a clear trend of stronger signal with increased Doppler shifts between the different heights in the atmosphere. We conclude that Doppler shifts of absorption profiles are responsible for the peaked PDF from our noiseless synthetic $B_{\text{app}}^{\text{L}}$. In effect, $|V_{\text{tot}}|$ is some combination of the vertical mean of B_z and the vertical mean of $|B_z|$ (depending on $v_z(z)$) and, consequently, the PDF of $B_{\text{app}}^{\text{L}}$ does not correspond to $\text{PDF}(B_z)$ from any geometrical height, optical depth, or volume. Such a failing of $B_{\text{app}}^{\text{L}}$ to accurately represent B_z cannot be captured using the Milne-Eddington approximation (used to calibrate $B_{\text{app}}^{\text{L}}$), which has no gradients by definition.

To examine the effect of noise on the PDF, we consider synthetic Stokes V profiles with noise added at a polarization precision of 1.1×10^{-3} (similar to that of the *Hinode* observations) in determining $B_{\text{app}}^{\text{L}}$. The PDF of this noisy synthetic observation is shown as a dotted line in Fig. 1 and closely resembles the observational PDF for signals weaker than a few Gauss. Note that, the noise accentuates the peak in the PDF even further. In examining Eq. (1) for V_{tot} ($B_{\text{app}}^{\text{L}}$ is a nearly-linear function of V_{tot}), we see that by taking the absolute value of the blue and red lobes separately the effect of noise becomes the sum of two non-negative measurement errors. That is,

$$V_{\text{tot}}^{\text{measured}} = V_{\text{tot}}^{\text{true}} + |\epsilon_b| + |\epsilon_r|, \quad (2)$$

where ϵ_b and ϵ_r are the measurement noise in the blue and red lobes (e.g., $\epsilon_b \equiv \sum_{i=1}^{N_b} \epsilon_i / N$ where ϵ_i are the random variables associated with the measurement noise in each wavelength bin). Assuming these two random variables, ϵ_b and ϵ_r have Gaussian distributions, their separate PDFs for their absolute values will peak at zero. However, the PDF of the sum of their absolute values will peak at a non-zero value due to reduced likelihood that $|\epsilon_b|$ and $|\epsilon_r|$ are small simultaneously: the PDF of the sum of two independent random variables is the convolution of their individual PDFs,

$$P(\epsilon) = \frac{2}{\pi \sigma_b \sigma_r} \int_0^\epsilon e^{-(\epsilon-\xi)^2/2\sigma_b^2} e^{-\xi^2/2\sigma_r^2} d\xi \quad (3)$$

for ϵ_b, ϵ_r Gaussian and $\epsilon = |\epsilon_b| + |\epsilon_r|$. Because of taking the absolute values, the individual PDFs are zero for negative values (this sets the limits of integration for Eq. (3)). Hence, their convolution is zero at zero and peaks instead for some finite positive value. Assuming ϵ_b and ϵ_r have identical standard deviation $\sigma = \sqrt{2} \cdot 2.4$ G (taken from Lites et al. 2008b), it can be shown that the peak in the PDF for $B_{\text{app}}^{\text{L}}$, Eq. (3), is given by the solution

to

$$\frac{B}{\sigma^2} \int_0^{B/2} e^{-\xi^2} d\xi - e^{-B^2/4} = 0. \quad (4)$$

This predicts a peak in the PDF at $B_{\text{app}}^L \approx 3 \text{ G}$, close to that seen in the actual observation. Consequently, adding noise leads to a further decrease of the number of pixels with very weak field and thus accentuates the maximum of the PDF. This illustrates that a monotonic $\text{PDF}(B_z)$ is qualitatively consistent with observations.

In Fig. 6, we use the 67.2 s exposure “deep mode” SP time series (dashed line). Note that for this exposure time, $\sigma = \sqrt{2} \cdot 0.6 \text{ G}$ (Lites et al. 2008b) and Eq. (4) predicts that the PDF will peak at $B_{\text{app}}^L \approx 1 \text{ G}$ (the actual peak is at $\approx 1.2 \text{ G}$). In this case, as in the “normal mode” case, the synthetic MURaM B_{app}^L with equivalent noise level (dotted line) matches the location of the peak and the PDF to the left of the peak. In fact, if we generate B_{app}^L from pure white noise for Stokes V (standard deviation of 3×10^{-4}), we find its PDF (plus signs) predicts well both the location of the peak and the shape of the weak-signal portion of the PDFs. This strongly suggests that the observational peak is dominated by noise.

We also find (see Fig. 6) that cancellation of opposite polarity fields in a resolution element alters the PDF and renders it useless for computations of the mean unsigned flux density and other moments. This is evidenced by a comparison of PDFs from the noisy synthetic MURaM B_{app}^L without (dotted line) and with spatial degradation by a theoretical point spread function (PSF, see Danilovic et al. 2008 for details) for *Hinode*’s optical system and rebinned to *Hinode* pixel size (diamonds). Because of the importance of the cancellation on the PDFs, PDFs may not be used to infer the true mean unsigned vertical flux density.

3.2. Cancellation

Turbulence gives rise to a statistically self-similar fractal pattern of the magnetic field (within the inertial range) – the field retains the same degree of complexity of distinct structures regardless of the scale at which it is observed (see, e.g., Constantin & Procaccia 1992; Brandenburg et al. 1992). In this section, we show that this also applies to solar surface magnetic fields and we use this self-similarity to estimate the portion of unsigned vertical flux unobservable at a given resolution. To begin with, we examine the cancellation properties of the magnetic field itself using a series of high-resolution MURaM dynamo simulations. This illustrates how the turbulent nature of the magnetic field limits measurement under the sole consideration of spatial resolution and in the absence of other observational constraints. As it separates the statistics of the field itself from observational constraints, the study also allows us to extrapolate the results to realistic solar magnetic Reynolds numbers.

Extending the ideas of singularity in probability measures for self-similar fractal fields to signed fields, Ott et al. (1992) introduced the *cancellation exponent* for studying the self-similar sign oscillations on very small scales in turbulent flows. For our application, their partition function, $\chi(l)$, measures the portion of the flux remaining after averaging over boxes of edge length l ,

$$\chi(l) \equiv \frac{\sum_i \left| \int_{\mathcal{A}_i(l)} B_z da \right|}{\int_{\mathcal{A}} |B_z| da} \quad (5)$$

where $\{\mathcal{A}_i(l)\} \subset \mathcal{A}$ is a hierarchy of disjoint subsets of size l covering the entire domain, \mathcal{A} . In our case, we call the function χ the *cancellation function* since it measures the flux cancellation at a given length-scale l . If the magnetic field is self-similar (for scales much larger than the dissipation scale), we expect a power-law

$$\chi(l) \propto l^{-\kappa}, \quad (6)$$

where κ is called the *cancellation exponent*. It is related to the characteristic fractal dimension of the magnetic field structures on all scales, D_f , by

$$\kappa = (d - D_f)/2 \quad (7)$$

where $d = 2$ is the embedding Euclidean dimension of the solar surface (Sorriso-Valvo et al. 2002).² An improved method to determine $\chi(l)$ using a Monte Carlo box counting technique was proposed by Cadavid et al. (1994). Its advantages include better counting statistics when l is a large fraction of the edge length of the domain \mathcal{A} , applicability to non-square pixels, and less sensitivity to the accidental placement of larger flux patches (e.g., network elements) with respect to the partitioning. For our simulation data, the Monte Carlo technique proved as accurate as rigid partition boxes but led to a significant reduction of the noise in $\chi(l)$: it averages over many partitionings and allows a more faithful representation of the field distribution (Cadavid et al. 1994). We use this technique for the results shown below.

The height range that corresponds (in a horizontally averaged sense) to $\log \tau \in [-2, 0.1]$ (as discussed in §3.1, the contribution for $\log \tau \in [-3.5, -2]$ to the Stokes V signal is insignificant) is $z \in [210, 300]$ km ($z = 0$ corresponds to the continuum optical depth $\tau = 1$ at 500 nm). For this height range we compute the averaged cancellation functions, $\chi(l)$, for MURaM dynamo simulations with magnetic Reynolds numbers ranging from $Re_M \approx 2000$ to

²Assuming the field is smooth (correlated) in D_f dimensions and uncorrelated in the other $d - D_f$ dimensions, the smooth dimensions contribute to the sum of vertical fluxes proportional to their area while the integral of an uncorrelated field contributes proportional to the square root of its area (random process). Eq. (7) then follows (Sorriso-Valvo et al. 2002).

$Re_M \approx 8000$. By definition, we have $\chi(l) = 1$ at the resolution of the simulation since there are no smaller scales for the computation. Furthermore, we expect dissipation to strongly affect $\chi(l)$ for the smallest decade of scales (analytically, its slope must go to zero). Also, as our dynamo simulations have zero signed total flux, $\chi(4.86 \text{ Mm}) = 0$ and we would expect scales down to approximately 490 km to be affected by this constraint. Only for smaller scales should we be able to observe a turbulent scaling. However, very little room is left between these two constraints so that no clear power-law scaling is observed for any of the simulations (see Fig. 7 for one example).

Since the dissipation scale of magnetic energy, l_η , decreases with increasing Re_M , for fixed l , $\chi(l)$ decreases with increasing magnetic Reynolds number (fluctuations at smaller scales increase the total cancellation). This is emphasized in Fig. 8, where we plot the value of the cancellation function for $l = 200 \text{ km}$ (corresponding roughly to *Hinode* SP’s angular resolution of $0''.3$) versus Re_M . We can fit a power law and extrapolate to the results we would expect from a MURaM simulation at solar Re_M (which must be estimated). From Kovitya & Cram (1983), we estimate the magnetic diffusivity for $\log \tau = 0$, $\eta \sim 10^8 \text{ cm}^2 \text{ s}^{-1}$. The driving of the small-scale dynamo is mainly subsurface where η is roughly 100 times smaller ($\eta \sim 10^6 \text{ cm}^2 \text{ s}^{-1}$, cf. Spruit 1974). For an upper limit of $\chi(200 \text{ km})$, we employ the more conservative estimate: $\eta \sim 10^8 \text{ cm}^2 \text{ s}^{-1}$. Taking the forcing scale to be the granulation scale, $\mathcal{L} \sim 1 \text{ Mm}$, and using $v_{rms} \sim 3 \text{ km s}^{-1}$ from the simulation, we find

$$Re_M \equiv \frac{\mathcal{L} v_{rms}}{\eta} \sim 3 \cdot 10^5. \quad (8)$$

For this magnetic Reynolds number, our extrapolation yields $\chi(200 \text{ km}) \sim 0.2$. This indicates that with a perfect observation at this spatial resolution and assuming that the MURaM simulation faithfully reproduces the solar conditions, we should multiply an observation by a factor of 5 to obtain the true mean vertical unsigned flux density of the quiet-Sun inter-network. It is also suggested by Fig. 8 that $\chi(200 \text{ km})$ decreases with decreasing magnetic Prandtl number, $P_M \equiv \nu/\eta$ where ν is the kinematic viscosity and η the magnetic diffusivity. As the magnetic Prandtl number of the Sun is much less than that of the simulations, we expect that $\chi(200 \text{ km}) \lesssim 0.2$.

The cancellation functions for B_z and for B_{app}^L inferred from Run C-NG are shown in Fig. 7. We see that the two functions are essentially equivalent. This demonstrates an excellent correspondence between the cancellation of the field itself and the signal derivable from observations (excluding instrumental effects). Therefore, we may take the cancellation of B_{app}^L as a proxy for the cancellation of B_z . This we now do.

We present the normalized cancellation function, $\chi(l)/\chi(1 \text{ Mm})$, for the *Hinode* SP observation in Fig. 9. Without knowing the value of the true unsigned vertical flux, the

denominator in Eq. (5), the value of the cancellation function can only be normalized to some arbitrary scale. We find a self-similar power-law over two decades in length scales, demonstrating the multifractal geometry of the turbulent quiet-Sun magnetic field. This is somewhat surprising as the dominant granulation pattern at scales near 1 Mm might have been expected to affect the cancellation scaling. The cancellation exponent of the scaling is $\kappa = 0.26 \pm 0.01$. This exponent predicts a 20% increase in the observed mean unsigned vertical flux density with a doubling of resolution in agreement with the difference in flux densities found between ground and space-based telescopes (Lites et al. 2008b). Note also that the power-law behavior holds down to the two-pixel scale. This is a clear indication of cancellation extending to smaller scales than resolved by *Hinode* (Carbone & Bruno 1997; Sorriso-Valvo et al. 2004). Compare this, for example, to the simulation case in Fig. 7 (also see Fig. 3(b) of Sánchez Almeida et al. 2003) where dissipation is seen to affect a strong turnover in $\chi(l)$ for the smallest decade of scales. As the observation is not so affected, we may safely conclude that the smallest scale of magnetic structuring is at least one decade smaller than the *Hinode* SP resolution limit. The scales of magnetic structuring in the photosphere must therefore extend to at least an order of magnitude smaller than 200 km.

From Eq. (7), we see that our result corresponds to $D_f = 1.48 \pm 0.02$ for the fractal dimension of the quiet Sun internetwork magnetogram. Within uncertainties, this is the same dimension as for solar plage regions, $D_f = 1.54 \pm 0.05$ (Balke et al. 1993). This might indicate that some similar mechanisms are at play in solar plage and quiet Sun internetwork. For the cancellation exponent of network magnetic fields, values of $\kappa \sim 0.4$ (Lawrence et al. 1993) and of $\kappa \sim 0.12$ (Cadavid et al. 1994) have been reported, but without an estimate of the uncertainties.

Recent work has highlighted the sensitivity of fractal dimension (perimeter-area) estimators to pixelization and resolution (Criscuoli et al. 2007). By using a signed measure, however, we avoid difficulties inherent to fractal dimension estimations using bi-level images in general and the perimeter-area method, specifically. Nonetheless, we have tested the sensitivity of the cancellation exponent to reducing our resolution by theoretical point spread functions for apertures 1/2 and 1/4 that of the *Hinode* SOT (50 cm). We find the slope of $\chi(l)$ to be robust in these cases for lengths exceeding 30 pixels. There is no change in the power law for almost one decade of length scales (3-20 Mm). We therefore conclude that our estimation, $\kappa = 0.26 \pm 0.01$ is robust and insensitive to pixelization and resolution effects. As pointed out by Lawrence et al. (1996), however, because of what they call “resolution-limited asymptotics”, different definitions of fractal dimension can give different values at finite resolution. For this reason, our value $D_f = 1.48 \pm 0.02$ might differ from a well-resolved perimeter-area estimate.

Using the self-similar power law derived from Fig. 9, we may estimate the true mean unsigned vertical component of the magnetic field (hereafter, “mean unsigned vertical flux density”) in the quiet-Sun photosphere, $\langle |B_z| \rangle$. Below the magnetic dissipation scale, l_η , there is no cancellation: $\chi(l_\eta) \equiv 1$. This, together with the self-similarity relation, Eq. (6), gives

$$\langle |B_z| \rangle = \langle |B_z| \rangle_{l_\eta} = \langle |B_z| \rangle_l \cdot \left(\frac{l}{l_\eta} \right)^\kappa, \quad (9)$$

where l is any scale in the inertial range, $\langle |B_z| \rangle_l$ is the mean absolute value of the vertical component of the field measured at that resolution (l),

$$\langle |B_z| \rangle_l \equiv \frac{\sum_i \left| \int_{\mathcal{A}_i(l)} B_z da \right|}{\int_{\mathcal{A}} da} = \chi(l) \cdot \langle |B_z| \rangle, \quad (10)$$

and $\langle |B_z| \rangle$ is given by

$$\langle |B_z| \rangle \equiv \frac{\int_{\mathcal{A}} |B_z| da}{\int_{\mathcal{A}} da}. \quad (11)$$

Lites et al. (2008b) report $\langle |B_z| \rangle_{0.11} \approx 11.7$ G. As $l \approx 0.11$ Mm (approximate *Hinode* SP pixel size) is below the SOT resolution limit, however, we rebin B_{app}^L to $l \approx 0.22$ Mm pixels to find $\langle |B_z| \rangle_{0.22} \approx 10.7$ G as the starting point of our estimate,

$$\langle |B_z| \rangle \approx 10.7 \text{ G} \cdot \left(\frac{0.22 \text{ Mm}}{l_\eta} \right)^{0.26}. \quad (12)$$

Estimating the magnetic dissipation scale is not straight-forward. As we have shown that observationally it is unresolved, we are left to rely on a phenomenological estimate. Kolmogorov phenomenology predicts (see, e.g., Frisch 1995) $l_\eta \approx \mathcal{L} Re_M^{-3/4}$ where \mathcal{L} is a large characteristic scale, such as the granulation scale. Using $Re_M \sim 3 \cdot 10^5$, derived previously, we estimate $l_\eta \sim 80$ m. For the dissipative range, power-law scaling for $\chi(l)$ will not apply and the slope of the cancellation function will approach zero. To provide a lower bound to the solar mean unsigned vertical field, we should then be conservative by ignoring any cancellation in the first decade of scales. Hence, we use $l_\eta = 800$ m in Eq. (12) to estimate the true mean unsigned vertical flux density to be $\langle |B_z| \rangle \gtrsim 46$ G. This means that, at a resolution of 200 km, at most one quarter of the unsigned vertical flux is observable.

4. Discussion

Our estimates suggest that three-quarters or more of the vertical unsigned magnetic flux is cancelled at the resolution of *Hinode*. Hanle-based estimates suggest $\langle |B| \rangle \sim 130$ G

(Trujillo Bueno et al. 2004)³ while Zeeman-based estimates suggest $\langle |B_z| \rangle \sim 10$ G (see Table 3 in Bello González et al. 2009). Note that even with estimation of the cancellation, there remains almost a factor of 3 difference between reported Hanle estimates and the Zeeman-based estimates we present. However, we have considered only one component of a vector quantity while the Hanle-based estimates are sensitive to the magnitude of that vector. Recent observations (Lites et al. 2008b) and simulations (Steiner et al. 2008; Schüssler & Vögler 2008) suggest that horizontal fields are on average a factor of 5 stronger than vertical fields. Therefore, our estimate of $\langle |B_z| \rangle \gtrsim 46$ G coupled with an even stronger mean horizontal field is consistent with the Hanle-based estimate. Another observational discrepancy lies in determining the mean “location” of the fields. Trujillo Bueno et al. (2004) interpret scattering polarization from molecular C_2 to indicate the mean field strength is weak (~ 10 G) over the bright granules, so that the turbulent field inferred from the Hanle measurements should be concentrated in the intergranular lanes. This should be compared to the location of strong horizontal fields not in the lanes but near the edges of granules (Lites et al. 2008b). In resolving the details over the location and strength of the mean components of the magnetic field, future work should also address the cancellation statistics of the horizontal field (and the linearly-polarized Stokes signals Q and U) as well as the effect on Stokes V presented here.

5. Conclusion

On the basis of surface dynamo simulations, we have demonstrated that the PDF generated from the Stokes V spectra are not necessarily equivalent in form to that of the PDF of the vertical component of the underlying magnetic field. The PDF for Stokes V shows a reduction of likelihood for weak vertical magnetic field compared to the PDF of the field itself. This effect is not due to a reduction in horizontal resolution, but is caused by a combination of vertical radiative transfer through a turbulent fluid (via the Doppler effect) and noise. That is, any systematic sampling (by geometrical height, optical depth, or volume) of B_z from the simulation yields a monotonic PDF, but due to Doppler shifts between different atmospheric heights, the Stokes V signal is not such a systematic sampling. Consequently, the PDF of Stokes V field estimates do not accurately represent the PDF of the actual vertical magnetic field even in the absence of noise. Additionally, for two different levels of noise (“normal mode” and “deep mode”) we have demonstrated that the peak in the observational

³Rather than assuming that a turbulent magnetic field possesses a delta-function PDF which leads to the ~ 60 G estimate in Trujillo Bueno et al. (2004), we take here the ~ 130 G estimate from their assumption of an exponential PDF.

PDF is dominated by the influence of noise. Because of these two effects, a monotonic PDF for the field can result in a peaked PDF in observations and the assumption that $\text{PDF}(B_z)$ can be uniquely derived from Stokes V observations becomes dubious.

From the cancellation function for a *Hinode* observation of the apparent longitudinal flux density, we have demonstrated that the multi-fractal self-similar pattern of the quiet-Sun photospheric magnetic field covers two decades of length scales down to the resolution limit, 200 km. This constitutes observational evidence that the smallest scale of magnetic structuring in the photosphere is at least an order of magnitude smaller than 200 km. The power law also allows us to constrain the quiet-Sun true mean unsigned vertical flux density. We estimate the lower bound to be ≈ 46 G. Estimates based solely on our numerical simulations suggest that the vertical unsigned flux at *Hinode*’s resolution should be multiplied by 5 to obtain the true vertical unsigned flux (i.e., ~ 50 G). These two results are consistent and suggest that the order of magnitude disparity between Hanle and Zeeman-based estimates may be fully resolved by a proper consideration of the cancellation properties of the full vector field.

Acknowledgments

The authors would like to acknowledge fruitful discussions with S. Solanki, A. Pietarila, and R. Cameron. *Hinode* is a Japanese mission developed and launched by ISAS/JAXA, collaborating with NAOJ as a domestic partner, NASA and STFC (UK) as international partners. Scientific operation of the *Hinode* mission is conducted by the *Hinode* science team organized at ISAS/JAXA. This team mainly consists of scientists from institutes in the partner countries. Support for the post-launch operation is provided by JAXA and NAOJ (Japan), STFC (U.K.), NASA, ESA, and NSC (Norway).

Note added in proof

We would like to point out the correlations between our conclusions and the works of Sanchez Almeida et al. (1996) and Sánchez Almeida & Lites (2000) who postulate structuring of the magnetic and velocity fields on scales much smaller than 100 km. They find that synthetic profiles generated by 3-component Milne-Eddington atmospheres re-produce the observed Stokes- V asymmetries found in $1''$ resolution observations. Though they did not estimate the undetected photospheric magnetic flux, the results indicated a significant fraction remaining undetected. Domínguez Cerdeña et al. (2006) assumed the quiet-Sun PDF can be approximated by a linear combination of the PDF inferred from Zeeman observations and a log-normal distribution (accounting for the observed Hanle depolarization). They determined that the Hanle and Zeeman signals are consistent with a single PDF with $\langle |B| \rangle \gtrsim 100$ G (see also Sánchez Almeida et al. 2003). Sánchez Almeida (2006) assuming

that numerical simulations of magnetoconvection with no dynamo action (20 km horizontal resolution) had achieved the asymptotic rate of magnetic energy dissipation, derived an estimate for the unsigned magnetic flux contained in unresolved scales; in our notation their finding is $\chi(100\text{ km}) \sim 0.5$ while our extrapolation estimates ~ 0.36 . Finally, Sánchez Almeida (2008) using observational data from various sources plot $\langle |B_z| \rangle_l$ versus l (their Fig. 1). The data are compared to a line, the slope of which corresponds to $\kappa = 1$, i.e., the result for white noise (Vainshtein et al. 1994, also set $D_f = 0$ in Eq. (7)). There is, however, a large scatter about this line suggestive of either a large uncertainty in κ or an element of randomness in the calibration issues between the various data used.

REFERENCES

- Balke, A. C., Schrijver, C. J., Zwaan, C., & Tarbell, T. D. 1993, *Sol. Phys.*, 143, 215
- Bello González, N., Yelles Chaouche, L., Okunev, O., & Kneer, F. 2009, *A&A*, 494, 1091
- Brandenburg, A., Procaccia, I., Segel, D., & Vincent, A. 1992, *Phys. Rev. A*, 46, 4819
- Cadavid, A. C., Lawrence, J. K., Ruzmaikin, A. A., & Kayleng-Knight, A. 1994, *ApJ*, 429, 391
- Carbone, V. & Bruno, R. 1997, *ApJ*, 488, 482
- Constantin, P. & Procaccia, I. 1992, *Phys. Rev. A*, 46, 4736
- Criscuoli, S., Rast, M. P., Ermolli, I., & Centrone, M. 2007, *A&A*, 461, 331
- Danilovic, S., Gandorfer, A., Lagg, A., Schüssler, M., Solanki, S. K., Vögler, A., Katsukawa, Y., & Tsuneta, S. 2008, *A&A*, 484, L17
- Domínguez Cerdeña, I., Sánchez Almeida, J., & Kneer, F. 2006, *ApJ*, 636, 496
- Frisch, U. 1995, *Turbulence, The Legacy of A. N. Kolmogorov* (Cambridge, UK: Cambridge University Press)
- Frutiger, C., Solanki, S. K., Fligge, M., & Bruls, J. H. M. J. 2000, *A&A*, 358, 1109
- Khomenko, E. V., Martínez González, M. J., Collados, M., Vögler, A., Solanki, S. K., Ruiz Cobo, B., & Beck, C. 2005, *A&A*, 436, L27

- Kosugi, T., Matsuzaki, K., Sakao, T., Shimizu, T., Sone, Y., Tachikawa, S., Hashimoto, T., Minesugi, K., Ohnishi, A., Yamada, T., Tsuneta, S., Hara, H., Ichimoto, K., Suematsu, Y., Shimojo, M., Watanabe, T., Shimada, S., Davis, J. M., Hill, L. D., Owens, J. K., Title, A. M., Culhane, J. L., Harra, L. K., Doschek, G. A., & Golub, L. 2007, *Sol. Phys.*, 243, 3
- Kovitya, P. & Cram, L. 1983, *Sol. Phys.*, 84, 45
- Krivova, N. A. & Solanki, S. K. 2004, *A&A*, 417, 1125
- Lawrence, J. K., Cadavid, A. C., & Ruzmaikin, A. A. 1996, *ApJ*, 465, 425
- Lawrence, J. K., Ruzmaikin, A. A., & Cadavid, A. C. 1993, *ApJ*, 417, 805
- Lites, B. W., Elmore, D. F., & Streander, K. V. 2001, in *Astronomical Society of the Pacific Conference Series*, Vol. 236, *Advanced Solar Polarimetry – Theory, Observation, and Instrumentation*, ed. M. Sigwarth, 33–+
- Lites, B. W., Ichimoto, K., Kubo, M., & et al. 2008a, *Sol. Phys.*, submitted
- Lites, B. W., Kubo, M., Socas-Navarro, H., Berger, T., Frank, Z., Shine, R., Tarbell, T., Title, A., Ichimoto, K., Katsukawa, Y., Tsuneta, S., Suematsu, Y., Shimizu, T., & Nagata, S. 2008b, *ApJ*, 672, 1237
- Orozco Suárez, D., Bellot Rubio, L. R., & del Toro Iniesta, J. C. 2007, *ApJ*, 662, L31
- Ott, E., Du, Y., Sreenivasan, K. R., Juneja, A., & Suri, A. K. 1992, *Physical Review Letters*, 69, 2654
- Sánchez Almeida, J. 2006, *A&A*, 450, 1199
- . 2008, *Ap&SS*, 156
- Sánchez Almeida, J., Emonet, T., & Cattaneo, F. 2003, *ApJ*, 585, 536
- Sanchez Almeida, J., Landi degl’Innocenti, E., Martinez Pillet, V., & Lites, B. W. 1996, *ApJ*, 466, 537
- Sánchez Almeida, J. & Lites, B. W. 2000, *ApJ*, 532, 1215
- Schrijver, C. J., Zwaan, C., Balke, A. C., Tarbell, T. D., & Lawrence, J. K. 1992, *A&A*, 253, L1
- Schüssler, M. & Vögler, A. 2008, *A&A*, 481, L5

- Socas-Navarro, H. & Sánchez Almeida, J. 2003, *ApJ*, 593, 581
- Solanki, S. K. 1987, PhD thesis, ETH Zürich
- Sorriso-Valvo, L., Carbone, V., Noullez, A., Politano, H., Pouquet, A., & Veltri, P. 2002, *Physics of Plasmas*, 9, 89
- Sorriso-Valvo, L., Carbone, V., Veltri, P., Abramenko, V. I., Noullez, A., Politano, H., Pouquet, A., & Yurchyshyn, V. 2004, *Planet. Space Sci.*, 52, 937
- Spruit, H. C. 1974, *Sol. Phys.*, 34, 277
- Steiner, O., Rezaei, R., Schaffenberger, W., & Wedemeyer-Böhm, S. 2008, *ApJ*, 680, L85
- Trujillo Bueno, J., Shchukina, N., & Asensio Ramos, A. 2004, *Nature*, 430, 326
- Tsuneta, S., Ichimoto, K., Katsukawa, Y., Nagata, S., Otsubo, M., Shimizu, T., Suematsu, Y., Nakagiri, M., Noguchi, M., Tarbell, T., Title, A., Shine, R., Rosenberg, W., Hoffmann, C., Jurcevich, B., Kushner, G., Levay, M., Lites, B., Elmore, D., Matsushita, T., Kawaguchi, N., Saito, H., Mikami, I., Hill, L. D., & Owens, J. K. 2008, *Sol. Phys.*, 249, 167
- Vainshtein, S. I., Sreenivasan, K. R., Pierrehumbert, R. T., Kashyap, V., & Juneja, A. 1994, *Phys. Rev. E*, 50, 1823
- Vögler, A. 2003, PhD thesis, Göttingen University
- Vögler, A., Bruls, J. H. M. J., & Schüssler, M. 2004, *A&A*, 421, 741
- Vögler, A. & Schüssler, M. 2007, *A&A*, 465, L43
- Vögler, A., Shelyag, S., Schüssler, M., Cattaneo, F., Emonet, T., & Linde, T. 2005, *A&A*, 429, 335

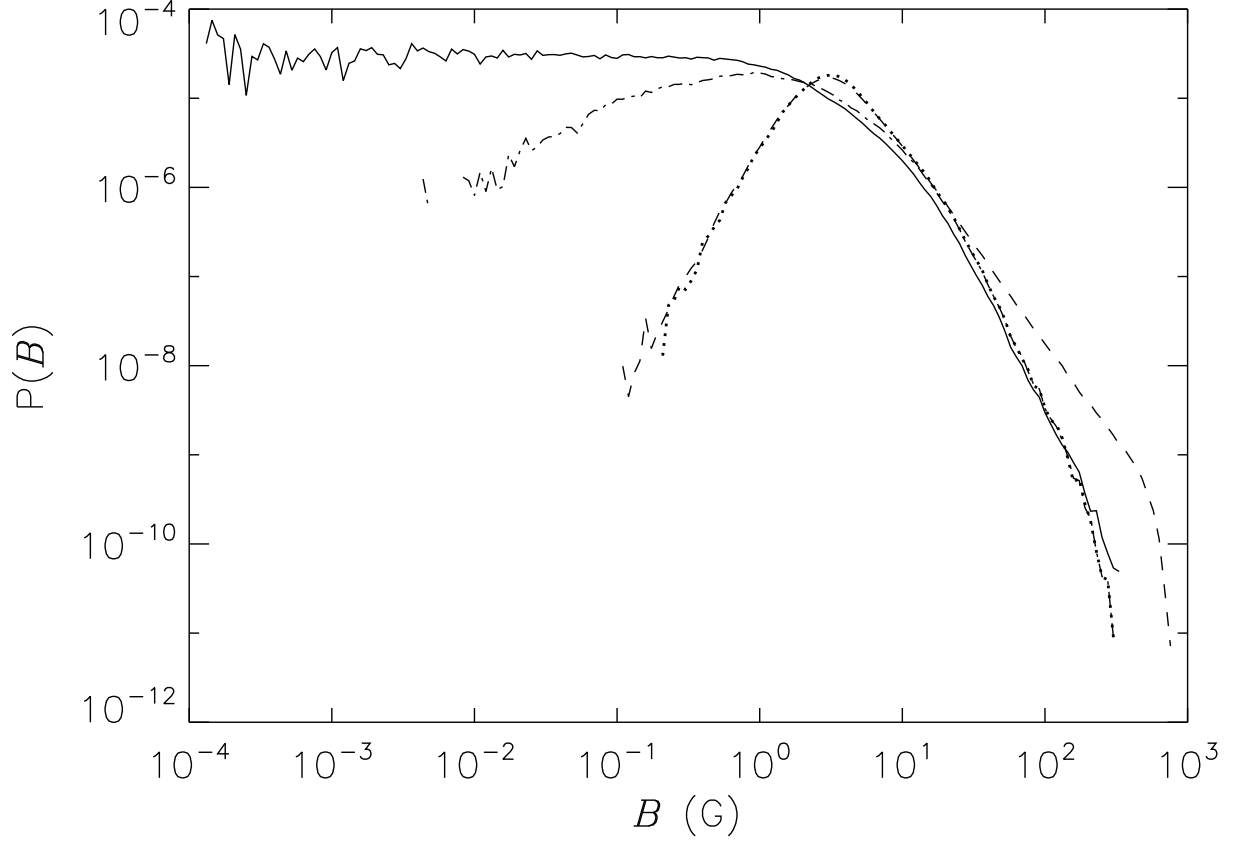


Fig. 1.— Probability distribution functions (PDFs) for magnetic field strengths and derived field proxies: *Hinode* SP “normal mode” map $B_{\text{app}}^{\text{L}}$ (dashed line), MURaM simulation B_{ave} (see text, solid line), MURaM synthetic $B_{\text{app}}^{\text{L}}$ (B derived from Stokes V , dot-dashed), and $B_{\text{app}}^{\text{L}}$ including a noise level of 1.1×10^{-3} (dotted). The PDFs of the synthetic observations appear peaked although we have a monotonic distribution of vertical field strengths.

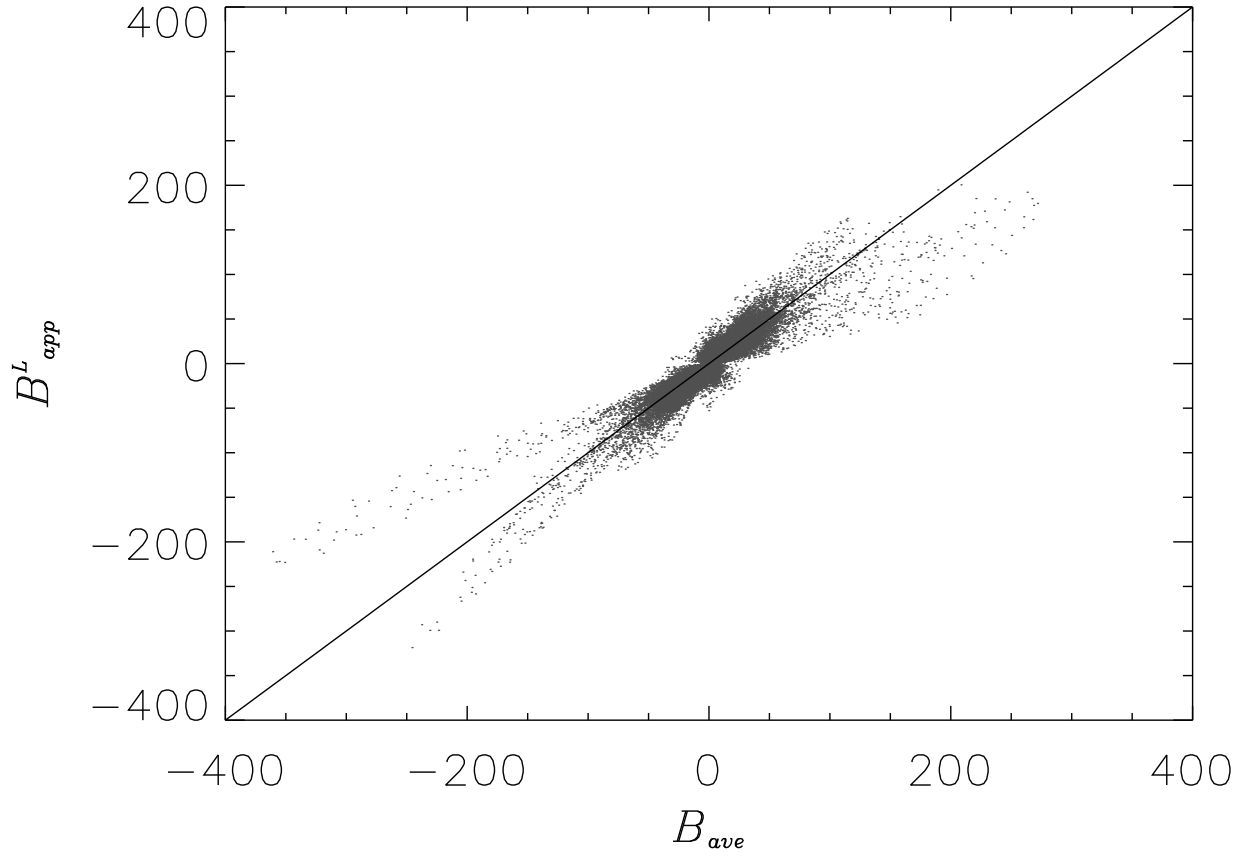


Fig. 2.— B_{app}^L derived from MURaM Run C-NG versus B_{ave} , the actual vertical magnetic field strength averaged over $\log \tau \in [-3.5, .1]$. The linear Pearson correlation for the two quantities is $r = 0.92$. Note the large scatter.

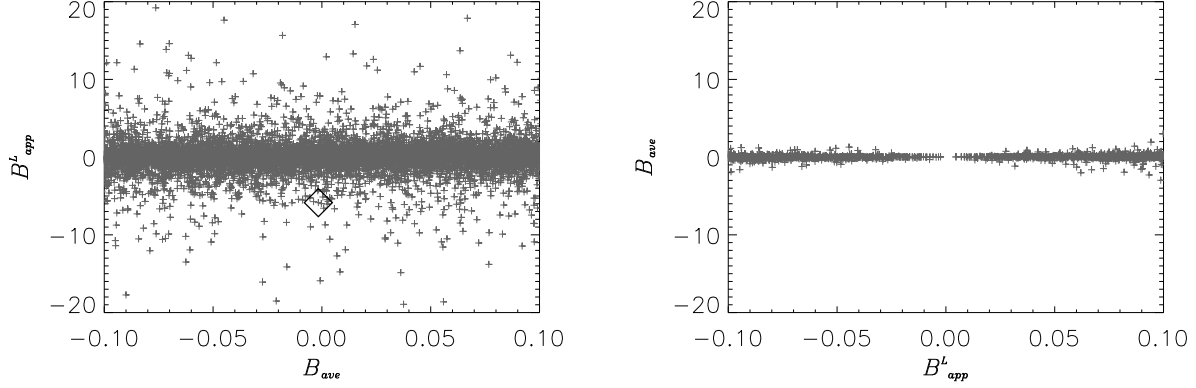


Fig. 3.— **(Left)** $B_{\text{app}}^{\text{L}}$ versus B_{ave} for $B_{\text{ave}} < 0.1$ G **(Right)** B_{ave} versus $B_{\text{app}}^{\text{L}}$ for $B_{\text{app}}^{\text{L}} < 0.1$ G ($B_{\text{app}}^{\text{L}}$ computed from noiseless V-profiles). These plots indicate the bias that strong Stokes V signal can be associated with a pixel with weak averaged magnetic field, but seldomly vice-versa.

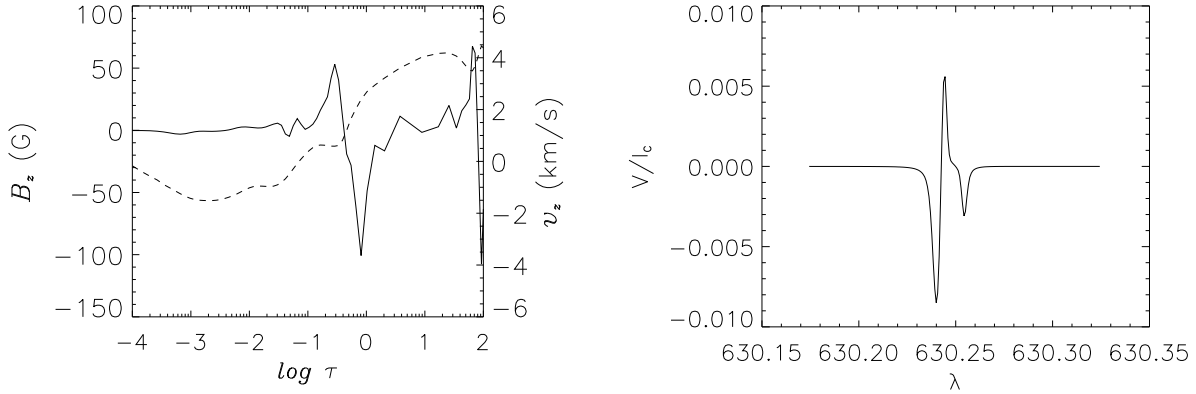


Fig. 4.— **(Left)** B_z (solid line) and v_z (dashed line) versus optical depth, $\tau_{500\text{nm}}$, and **(Right)** Stokes V profile for the pixel indicated by a diamond in Fig. 3 ($B_{\text{app}}^{\text{L}} = -5.9$ G and $B_{\text{ave}} = -1.6 \cdot 10^{-3}$ G). At $\log \tau = 0$ the positive and negative contributions to B_{ave} have nearly cancelled (integrating downward). The Stokes V signal is stronger than would result from a uniform $1.6 \cdot 10^{-3}$ G field but is asymmetric. Strong gradients lead to asymmetric profiles but also to $|B_{\text{app}}^{\text{L}}| \gg |B_{\text{ave}}|$.

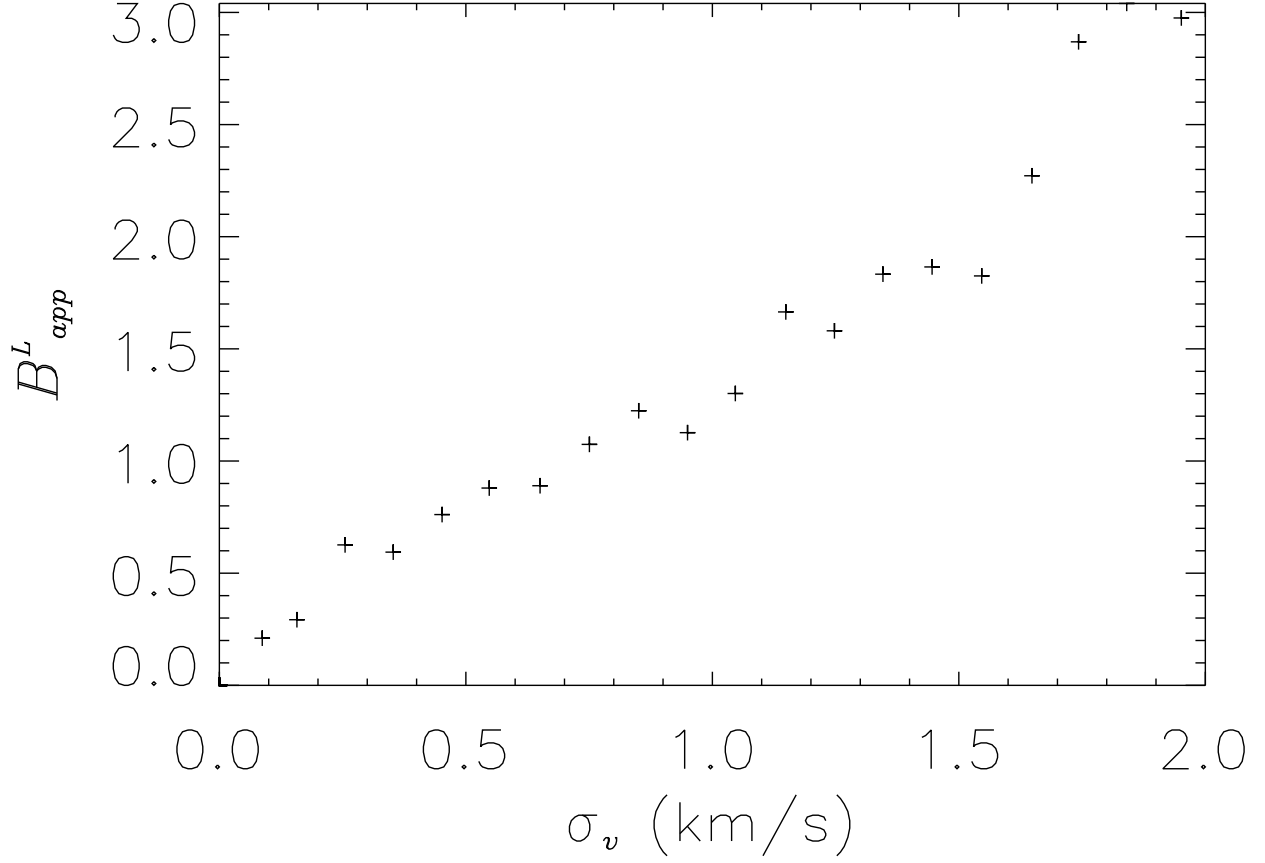


Fig. 5.— Average B_{app}^L versus standard deviation of the fluctuations of the vertical velocity along the (vertical) line-of-sight, σ_v , for all pixels with $|B_{ave}| < 0.1$ G. Pixels are binned by σ_v before averaging. With strong velocity differences between different heights in the atmosphere, the total Stokes V signal increases as the Doppler-shifted absorption from positively and negatively oriented fields show less cancellation.

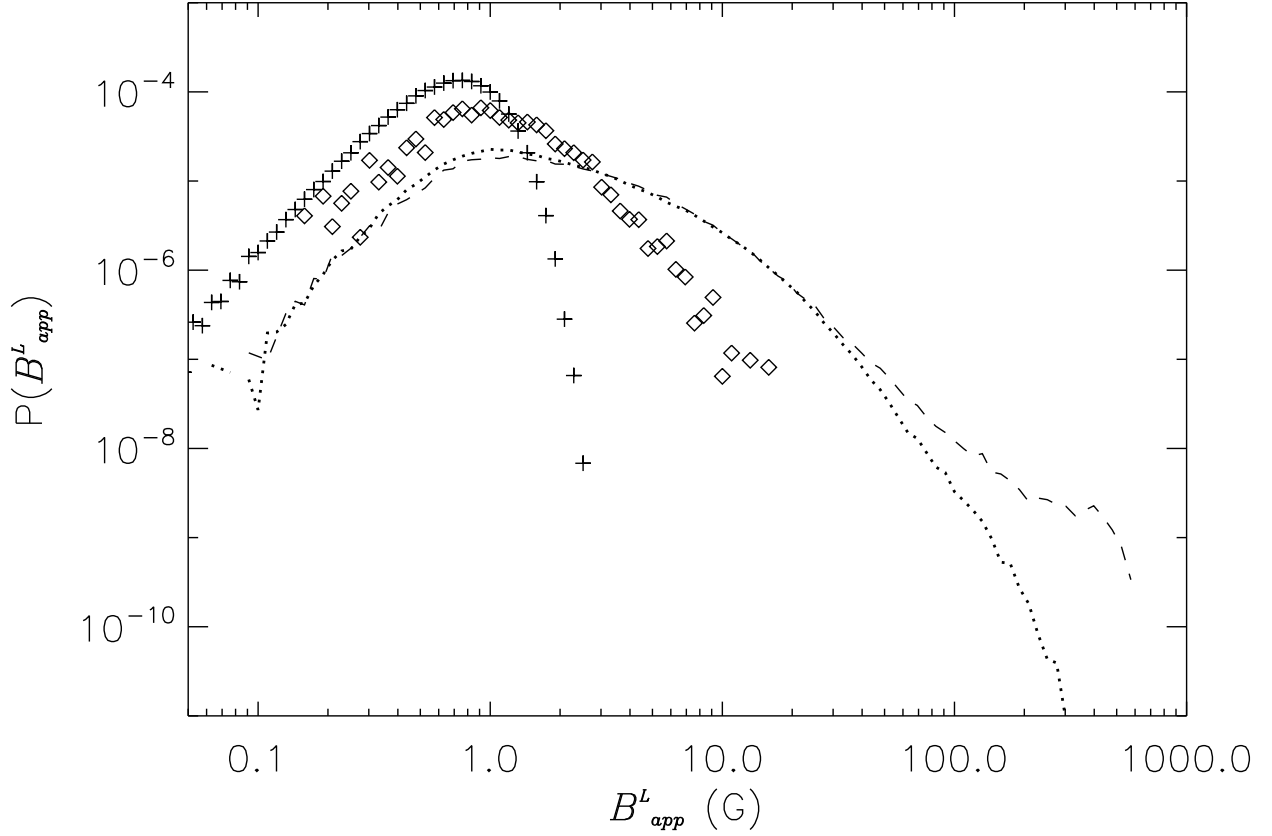


Fig. 6.— PDFs for derived field proxies: *Hinode* SP “deep mode” time series B_{app}^L (dashed line) and **MURaM** synthetic B_{app}^L including a noise level of 3×10^{-4} (dotted). The effects of cancellation due to finite spatial resolution are seen in the PDF of the synthetic signal including noise as well as spatial smearing from a theoretical PSF and rebinning to *Hinode* resolution (diamonds). As this represents a real loss of data, the true mean unsigned vertical flux density cannot be calculated from the observational PDF. Also shown is the result for employing pure white noise with a standard deviation of 3×10^{-4} for Stokes V (+).

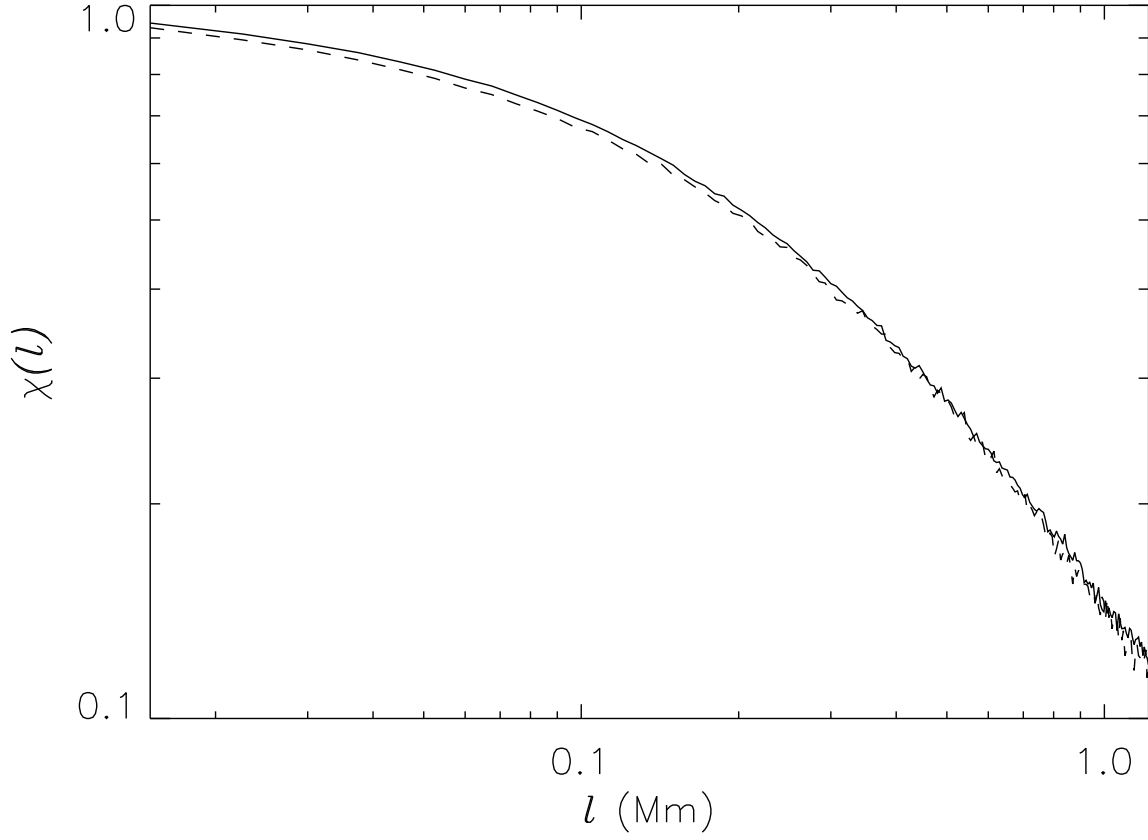


Fig. 7.— Cancellation function, $\chi(l)$, versus scale, l for Run C-NG: B_z (solid line) and B_{app}^L (simulated observation, dashed). The two are essentially equivalent, suggesting that the cancellation of B_{app}^L may be taken as a proxy for the cancellation of B_z .

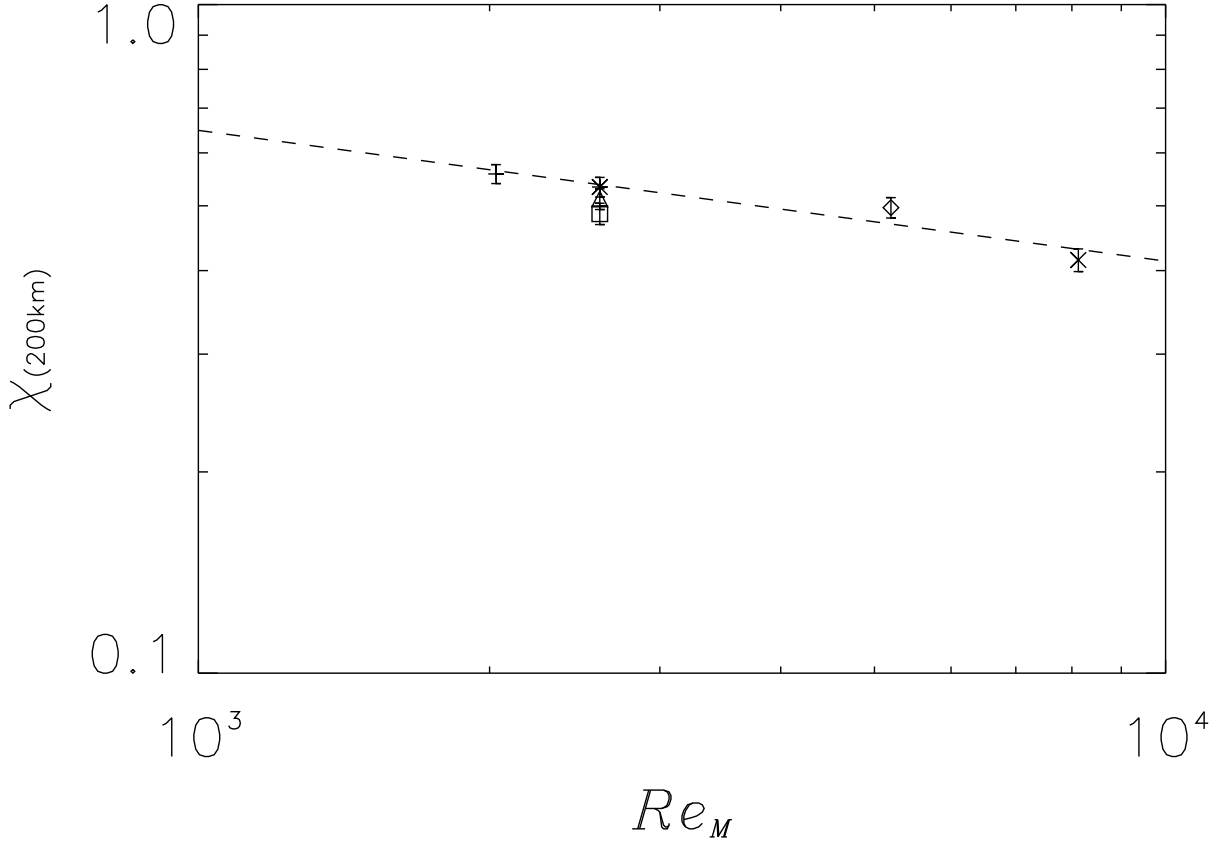


Fig. 8.— Portion of flux remaining at $l = 200$ km, $\chi(200\text{ km})$, versus magnetic Reynolds number, Re_M . Symbols are Run E (plus), Run C (asterisk), Run G (diamond), Run H (X), Run C-NG (triangle), and Run G-P (square)—see Table 1. For fixed l , $\chi(l)$ decreases with Re_M and shows an approximate power-law relation with Re_M as indicated by the fitted dashed line. Run C-NG and Run G-P are not included in the fit, but the effect of decreased magnetic Prandtl number leads to reduced $\chi(200\text{ km})$. Taking this into consideration, along with extrapolation to solar values, $Re_M \sim 3 \cdot 10^5$, we estimate $\chi(200\text{ km}) \lesssim 0.2$.

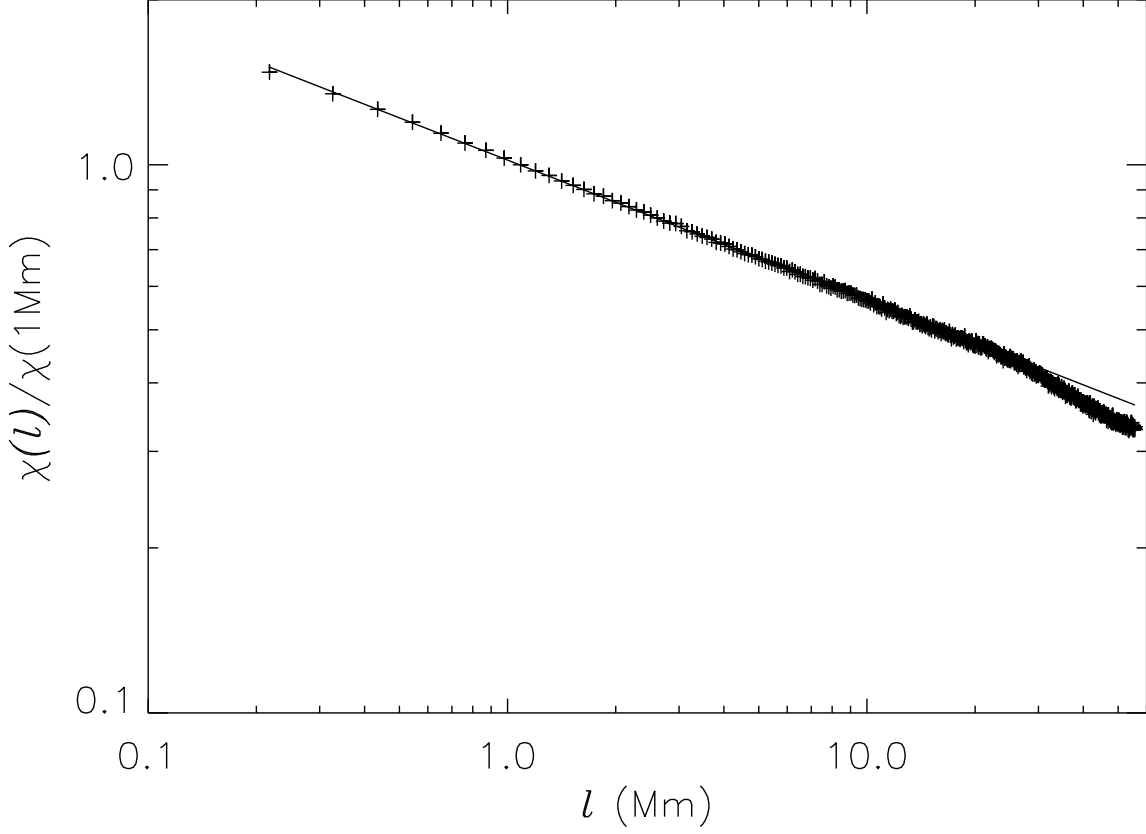


Fig. 9.— Normalized cancellation function, $\chi(l)/\chi(1 \text{ Mm})$, versus scale, l , from *Hinode* $B_{\text{app}}^{\text{L}}$ observation. A self-similar power-law is abundantly clear for 2 decades of length scales down to the resolution limit of the observation (the fitted line is $k = 0.26 \pm 0.01$). This indicates both the possibility for self-similar extrapolation to smaller scales and that the smallest scales of magnetic structuring must be at least an order of magnitude smaller than 200 km.

Table 1. Summary of MURaM simulation runs: shown are grid points, horizontal resolution, and magnetic Reynolds number, Re_M . All runs except Run C-NG utilize grey radiative transfer. In Run C-NG, opacity binning with 4 bins (Vögler et al. 2004) has been used to provide non-grey radiative transfer. For all simulations no physical viscosity is imposed. Rather, numerical dissipative effects lead to an effective kinetic Reynolds number, Re (Vögler et al. 2005). To obtain a lower value of $P_M = Re_M/Re$, Run G-P uses the magnetic diffusivity used in Run C but at a higher resolution, hence higher Re .

Simulation	Computational Grid	Horizontal Resolution	Re_M
Run E	$540 \times 540 \times 140$	9 km	≈ 2000
Run C	$648 \times 648 \times 140$	7.5 km	≈ 2600
Run C-NG	$648 \times 648 \times 140$	7.5 km	≈ 2600
Run G-P	$972 \times 972 \times 200$	5 km	≈ 2600
Run G	$972 \times 972 \times 200$	5 km	≈ 5200
Run H	$1215 \times 1215 \times 350$	4 km	≈ 8100